

Resource Requirements for Fault-Tolerant Quantum Simulation: The Transverse Ising Model Ground State

Craig R. Clark and Kenneth R. Brown*

*School of Chemistry and Biochemistry and Division of Computational Science and Engineering,
Georgia Institute of Technology, Atlanta, GA 30332-0400*

Tzvetan S. Metodi and Samuel D. Gasster

Computer Systems Research Department, The Aerospace Corporation, El Segundo, CA 90245-4691

(Dated: May 29, 2019)

The cost, in both computational space and time, of calculating the energy of the ground state of the transverse Ising model on a fault-tolerant quantum computer is estimated using the Quantum Logic Array (QLA) architecture model. The QLA is a homogeneous, scalable, tile-based quantum architecture design employing concatenated quantum error correction for the construction of logical qubits and gates, based on experimentally viable ion-trap device technology parameters and components. The error correction requirements for calculating the energy on the QLA architecture are comparable to those for factoring large integers via Shor's quantum factoring algorithm number due to the exponential scaling of the computational timesteps with the precision. As a result, a fault-tolerant QLA-based quantum computer which can factor 1024-bit integers can also be used to calculate the Ising ground-state energy with precision of up to 7 decimal digits.

I. INTRODUCTION

The calculation of the basic quantum system properties (eigenstates and eigenvalues) remains a challenging problem for computational science. One of the most significant issues is the exponential scaling of the computational resource requirements with the number of particles and degrees of freedom, which for even a small number of particles (~ 100) exceeds the capabilities of current computer systems. In 1982 Feynman addressed this problem by proposing that it should be possible to use one quantum system as the basis for the simulation of another [1]. This was the early promise of quantum simulation, and one of the original motivations for quantum computing. Since that time, many researchers have investigated different approaches to quantum simulations [2, 3, 4, 5, 6, 7]. For example, Abrams and Lloyd have proposed a quantum algorithm for the efficient computation of eigenvalues and eigenvectors using a quantum computer

*Electronic address: ken.brown@chemistry.gatech.edu

[4]. Many of these papers consider ideal components providing an optimistic perspective on the resource requirements for implementing quantum simulations and computations. However, when one accounts for the effects of decoherence and technical limitations in the implementation of quantum computing components, a fault-tolerant approach becomes necessary[8, 9].

The main goal of this paper is to evaluate the quantum simulation/computation resource requirements in the context of a fault-tolerant quantum computer architecture. The general approach of Abrams and Lloyd [3, 4] for estimating the ground state energy is analyzed in a fault-tolerant framework. The logical quantum circuit for eigenvalue estimation is encoded into a physical layer based on a fault-tolerant protocol using well known quantum error correcting codes [9, 10, 11, 12, 13]. Implementation of a fault-tolerant quantum simulation requires additional quantum resources relative to an ideal error free implementation. We present here an estimate for the total number of qubits required for a fault-tolerant implementation, and the number of quantum operations at both the logical and physical level.

The resource analysis is performed in the context of a specific quantum simulation problem: computing the ground state energy of the Transverse Ising Model (TIM). The relevant details of the TIM are described in Section II. In Section III, we show how the calculation of the TIM ground state energy is mapped onto the phase estimation algorithm. The required unitary transformations are decomposed into one qubit gates and two-qubit controlled-not gates using gate identities and the Trotter formula. The one-qubit gates are approximated by a set of gates which can be executed fault-tolerantly using the Solovay-Kitaev theorem [14]. The results of Section III are independent of architecture and reflect the number of high-level timesteps necessary to implement the phase estimation circuit fault-tolerantly.

In Section IV, the fault-tolerant circuit is mapped onto the Quantum Logic Array (QLA) architecture model [15]. The QLA was originally developed assuming the performance capability of ion trap based qubits in a series of interconnected traps. The QLA architecture may be applied to any two-dimensional array of qubits where the qubits are physically moved between locations on a timescale comparable to, or longer than, the time to execute a single qubit gate operation. The fault-tolerant gate operations, described in Section III, are described in terms of a series of physical operations within the QLA architecture. The QLA architecture is summarized in Appendix A.

In Section V, the results of the resource analysis are compared with the resource requirements for a QLA implementation of Shor's algorithm [15]. Section VI contains the conclusions and possible approaches to improving the performance for quantum simulation applications.

II. TRANSVERSE ISING MODEL

The Transverse Ising Model is used for the analysis of the resource requirements for quantum simulation and computation. The TIM is one of the simplest models exhibiting a quantum phase transition at zero temperature [16, 17, 18, 19]. The calculation of the ground state energy of the TIM varies from analytically solvable in the linear case [16] to numerically difficult for frustrated 2D lattices [20, 21]. For example, the calculation of the magnetic behavior of frustrated Ising antiferromagnets requires computationally intensive Monte-Carlo simulations [22]. Given the difficulty of the generic problem and the centrality of the TIM to studies of quantum phase transitions and quantum annealing, the TIM is a good benchmark model for quantum computation studies.

The Transverse Ising Model consists of a set of N -spin-1/2 particles at each site of a D -dimensional lattice. The TIM Hamiltonian H_I may be written as [19]:

$$H_I = \sum_i \Gamma \sigma_i^x + \sum_{\langle i,j \rangle} J_{ij} \sigma_i^z \sigma_j^z, \quad (1)$$

where J is the spin-spin interaction energy, Γ is the coupling constant and related to the strength of the external magnetic field along the \hat{x} -direction, and $\langle i, j \rangle$ implies a sum only over nearest-neighbors. σ_i^x and σ_i^z are the Pauli spin operators for the i th spin. We assume $\hbar = 1$ throughout this paper.

In the remainder of this paper, we focus on the specific case of a linear chain TIM of N spins with constant Ising interaction energy $J_{ij} = -J$. The geometry of this model is shown in Figure 1. The ground state of the system is determined by the ratio of $\Gamma/J = g$. For the large magnetic field case, $g \gg 1$ the system is paramagnetic with all the spins aligned along the \hat{x} axis. In the limit of small magnetic field, $g \ll 1$, the system has two degenerate ferromagnetic ground states, parallel and anti-parallel to the \hat{z} axis. In the the intermediate range of magnetic field strength the linear TIM exhibits a quantum phase transition at $g = 1$ [19].

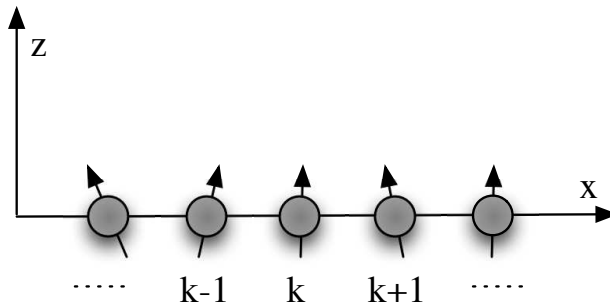


FIG. 1: The 1-D Transverse Ising Model.

The TIM Hamiltonian, Equation 1, for the 1-D case with constant coupling can be rewritten as

$$H_I = -J \left(\sum_i g X_i + \sum_{i,j=i+1} Z_i Z_j \right) \quad (2)$$

where the Pauli spin operators are replaced with their corresponding matrix operators X_i, Z_i . For the 1-D TIM, the ground state energy can be calculated analytically in the limit of large N . In the case of a finite number of spins with non-uniform spin-spin interactions (J not constant), it is possible to efficiently simulate the TIM using either the Monte-Carlo method [23] or the density matrix renormalization group approach [24]. The challenge for classical computers comes from the 2-D TIM on frustrated lattice, whose simulation scales exponentially with N . On the other hand, as we shall see in Sections III, IV, and V, applying the quantum phase estimation circuit to calculate the ground state energy of the TIM problem requires physical qubit resources which scale polynomially with N and number of computational timesteps which are largely independent with N . In addition, just as the complexity of the problem is independent of the lattice dimension and layout when applying classical brute force diagonalization, the cost of applying the quantum phase estimation circuit is largely independent of the dimensionality of the TIM Hamiltonian.

III. DECOMPOSITION OF THE CIRCUIT FOR CALCULATING THE TIM GROUND-STATE ENERGY

In this section we map the problem of computing the ground state energy for the TIM Hamiltonian in Equation 2 to the phase estimation circuit following the Abrams and Lloyd quantum phase estimation algorithm [3, 4]. We specifically describe how the circuit relates to the number of bits of precision in the final estimate of the energy and calculate the total number of timesteps and qubits required to implement the circuit. To implement the operation in the circuit fault-tolerantly, we decompose each operation into a set of gates which can be implemented fault-tolerantly using the error correcting codes in the QLA architecture. The set of gates consists of the Hadamard gate (denoted with H), the two-qubit controlled-not gate (denoted as the CNOT gate), the single-qubit T and S gates which are rotations around the \hat{z} -axis by $\pi/8$ and $\pi/4$ radians respectively, and the measurement gate. The cost of the circuit is calculated based on the resulting decomposition to accurately represent the resource requirements of the circuit in a fault-tolerant environment.

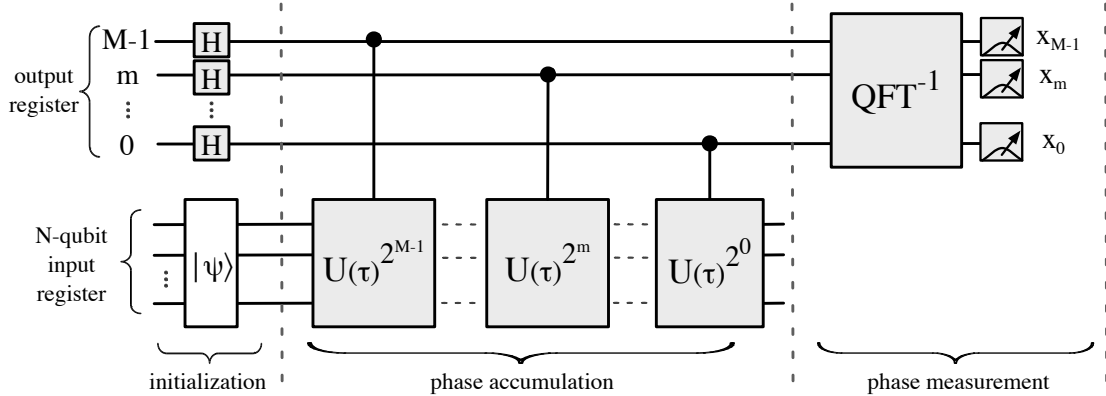


FIG. 2: The phase estimation circuit used to calculate the ground-state energy of the d -Dimensional TIM problem. The letter m denotes the m th qubit in the output register, where $0 \leq m \leq M - 1$.

A. Overview of the circuit for the TIM problem

The circuit for the TIM problem is shown in Figure 2. It consists of an N -qubit *input* quantum register corresponding to the N spin-1/2 particles representing the size of the problem and an M -qubit *output* register used for storing the result. The circuit in Figure 2 can be divided into three distinct steps: initialization, phase accumulation, and phase measurement.

The initialization step initializes the input and output quantum registers. The M -qubit output register is initialized into an equal superposition of all numbers between 0 and $(2^M - 1)$ via M Hadamard gates applied in parallel to each qubit. The input register is prepared in an initial quantum state $|\Psi\rangle$, which is an approximation to the ground-state $|\Psi_g\rangle$ of the TIM Hamiltonian H_I . For the TIM this can be accomplished using classical approximation techniques to calculate an estimated wavefunction or adiabatic quantum state preparation techniques [6]. The overlap between $|\Psi\rangle$ and $|\Psi_g\rangle$, given by $|\langle\Psi|\Psi_g\rangle|^2$, is the probability that the result after measuring the output register at the end of the circuit will allow us to correctly compute the ground-state energy [4]. Thus, the closer the initial state $|\Psi\rangle$ is to the ground-state $|\Psi_g\rangle$ the more likely the computation will successfully lead to the ground-state energy. The preparation of an approximation to $|\Psi_g\rangle$ for generic Hamiltonians consisting of two spin interactions is quite difficult [25, 26] but the phase-estimation algorithm is of comparable complexity as described in Section V. Consequently for the remainder of this paper, we do not consider the cost of preparing the initial state $|\Psi\rangle$. The focus is on the computational cost of calculating the ground-state energy via the circuit in Figure 2 given $|\Psi\rangle$.

The key to the phase accumulation step of the circuit in Figure 2 is the unitary operator $U(\tau) = e^{iH_I\tau}$ with eigenvalue $e^{2\pi i\phi}$. As shown in the figure, repeated powers of $U(\tau)$ are applied on the input quantum

register controlled on each successive qubit in the output register. At the completion of the phase accumulation step, the output register is the quantum Fourier transform (QFT) of the M -bit estimate of the phase ϕ of an eigenvalue of $U(\tau)$ [27].

The phase measurement step of the circuit is where ϕ 's M -bit estimate is extracted from the state of the output register in order to calculate E . The step consists of the M -qubit inverse quantum Fourier transform (QFT), followed by measurement of each of the M qubits. After applying the QFT, the state of the output register becomes $|x_1 x_2 \dots x_M\rangle$, where $x_m \in \{0, 1\}$ corresponds to the state of the m th qubit. Measuring each qubit yields the M -bit binary bitstring “ $x_1 x_2 \dots x_M$ ”, which corresponds to the M -bit approximation of ϕ given by $\tilde{\phi} = 0.x_1 \dots x_M$ in binary notation. Using the estimate of ϕ , the energy, $E = \frac{2\pi\phi}{\tau}$, can be calculated. It will correspond to the ground-state energy E_g with probability equal to $|\langle \Psi | \Psi_g \rangle|^2$.

When setting the parameter τ in the definition of $U(\tau)$, we must consider that the result of the phase estimation circuit is the binary fraction $0.x_1 \dots x_M$, which is less than one [3, 4]. Thus, to ensure that this value is a valid approximation of the phase ϕ , we must set the parameter τ such that $\tau < 2\pi/E_g$, which corresponds to $\phi < 1$. In the case of a linear TIM, $|E_g|$ is bounded by $NJ(1 + g)$ [16]. Thus in the region near the phase transition $g \approx 1$, setting τ to $1/(10JN)$ satisfies both $|E_g| < NJ(1 + g)$ and the condition that $\phi < 1$.

B. Decomposing the Phase Accumulation Step in the TIM Circuit

The first step of the TIM circuit that needs to be decomposed into H , T , S , and CNOT gates is the phase accumulation step. As shown in Figure 2, the phase accumulation step consists of M N -qubit controlled unitary gates, where the m th N -qubit unitary (given by $U(\tau)^{2^m}$) is controlled on the m th qubit in the output register. Substituting for the TIM Hamiltonian in the expression for the unitary $U(\tau)^{2^m}$ for some arbitrary $m < M$, we can express $U(\tau)^{2^m}$ as:

$$U(\tau)^{2^m} = e^{-i(2^m\tau)H_I} = U(2^m\tau) = \exp\left(-i(2^m\tau)\left[-J\left(g\sum_i X_i + \sum_{i,j=i+1} Z_i Z_j\right)\right]\right), \quad (3)$$

Since decomposing $U(2^m\tau)$, as written in Equation 3, is difficult, we can use the Trotter formula [28] to approximate it as a product of unitary operators U_x and U_{zz} , which are the two non-commuting components of the Hamiltonian H_I . These operators correspond to the evolution of the system under the magnetic field and the Ising interaction and can be further decomposed independently. Using the Trotter formula, the approximation for $U(2^m\tau)$ can be written as:

$$\begin{aligned}
U(2^m \tau) &= \tilde{U}(2^m \tau) + \epsilon_T \\
&= [U_x(\Gamma\theta) U_{zz}(J2\theta) U_x(\Gamma\theta)]^k + \epsilon_T
\end{aligned} \tag{4}$$

where $k \geq 1$ is the integer Trotter parameter, $\theta = (2^m \tau/k)$, and ϵ_T is the Trotter approximation error. As a function of θ , the evolution under the magnetic field $U_x(\Gamma\theta)$ and the Ising interaction $U_{zz}(J2\theta)$ are given by:

$$U_x(\theta) = \prod_{j=0}^{N-1} \exp(-i \frac{\Gamma\theta}{2} X_j) \tag{5}$$

$$U_{zz}(2\theta) = \prod_{i,j=0,i+1}^{N-1} \exp(-iJ\theta Z_i Z_j) \tag{6}$$

For fixed $|J| + |\Gamma|$, the Trotter error ϵ_T is maximized for $J = \Gamma = 1$ corresponding to the critical $g = g_c = 1$, representing a worst-case scenario for the algorithm. We calculate the resource requirements at this critical point and assume that $J = \Gamma = 1$ for the remainder of this paper. The integer Trotter parameter k is determined via the magnitude of ϵ_T , which scales as $O\left(N \frac{(2^m \tau)^3}{k^2}\right)$ [29]. Thus, as k increases the Trotter error decreases. Since ϵ_T must be smaller than the energy precision $(2\pi/2^M \tau)$, k is incremented until $\epsilon_T < (2\pi/2^M \tau)$. The Trotter parameter k scales as:

$$k = O\left(\sqrt{\frac{2^{M+3m}}{N^3}}\right), \tag{7}$$

where for small m such that the fraction in the equation above is less than unity, the parameter k is simply one. In Section V, k is numerically calculated for specific examples of the TIM problem and verified to scale exponentially with m . In addition, the fact that k scales approximately as $1/N$ can be attributed to the fact that the angle θ in the Trotter approximation is proportional to τ , which is proportional to $1/N$. The N dependence is unimportant relative to the scaling with precision as shown in Section V.

To see the dependence of the number of timesteps necessary to implement the controlled- $U(2^m \tau)$ operator on the Trotter parameter k , we can expand Equation 4 and write $\tilde{U}(2^m \tau)$ as:

$$\tilde{U}(2^m \tau) = U_x(\theta)(U_{zz}(2\theta)U_x(2\theta))^{k-1}U_{zz}(2\theta)U_x(\theta) \tag{8}$$

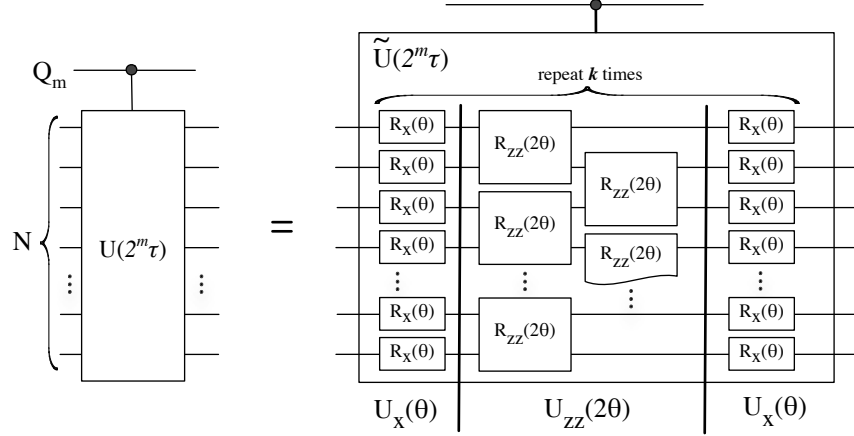


FIG. 3: The Trotter circuit which approximates a given $U(2^m \tau)$ applied on all N input Ising qubits and controlled on the m th output qubit Q_m .

Thus, approximating $U(2^m \tau)$ will require the sequential implementation of k controlled- $U_{zz}(2\theta)$ gates, $(k - 1)$ controlled- $U_x(2\theta)$ gates, and two instances of controlled- $U_x(\theta)$ gates, all controlled on the m th output qubit in the output quantum register.

The circuit for the controlled- $\tilde{U}(2^m \tau)$ is shown in Figure 3, which reflects its implementation using the Trotter formula by illustrating the evolutions under the magnetic field $U_x(\theta)$ and the Ising interaction $U_{zz}(2\theta)$. As shown in the right-hand-side of the figure, $U_x(\theta)$ can be described as the unitary operator $R_x(\theta)^{\otimes N}$ where $R_x(\theta) = \exp(-i\frac{\theta}{2}X)$ is a single qubit rotation about the \hat{x} axis, applied to each of the N qubits in the input register. Similarly, $U_{zz}(2\theta)$ can be built from the two qubit rotations $R_{zz}(2\theta) = \exp(-i\theta ZZ)$ applied pairwise on all the qubits from the input register. Expanding the right-hand-side of Figure 3 to reflect Equation 8 will give us a circuit gate sequence given by: $\{U_x(\theta), U_{zz}(2\theta), U_x(2\theta), \dots, U_{zz}(2\theta), U_x(\theta)\}$.

Since $U_x(\theta)$, $U_x(2\theta)$, and $U_{zz}(2\theta)$ are *controlled* operators, each of the individual $R_x(\theta)$, $R_x(2\theta)$, and $R_{zz}(2\theta)$ gates are also multi-qubit controlled gates and must be expressed in terms of single-qubit $R_z(\theta) = \exp(-i\theta Z)$ gates and CNOT gates. This is accomplished with two identities: (1) $R_x(\theta) = HR_z(\theta)H$, and (2) $R_z(\theta) = R_z(\theta/4)XR_z^\dagger(\theta/2)XR_z(\theta/4)$ described in Reference [28], where the gate R_z^\dagger is the complex conjugate of R_z . Single-qubit R_z gates can be approximated efficiently using H , T , T^\dagger , and S gates using the Solovay-Kitaev theorem [14], and thus can be implemented fault-tolerantly with the QLA architecture when error correction is needed.

Using the above identities, Figure 4 illustrates the transformation of the controlled- $U_x(\theta)$ gate into single-qubit $R_z(\theta/4)$, $R_z^\dagger(\theta/2)$, and CNOT gates. In the construction of the Figure 4 circuit, $(N - 1)$

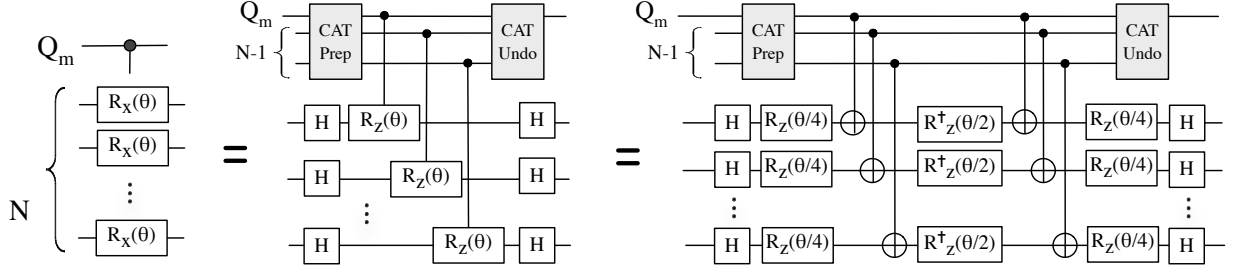


FIG. 4: The decomposition of the controlled unitary operation $U_x(\theta)$ into single-qubit R_z gates and CNOT gates.

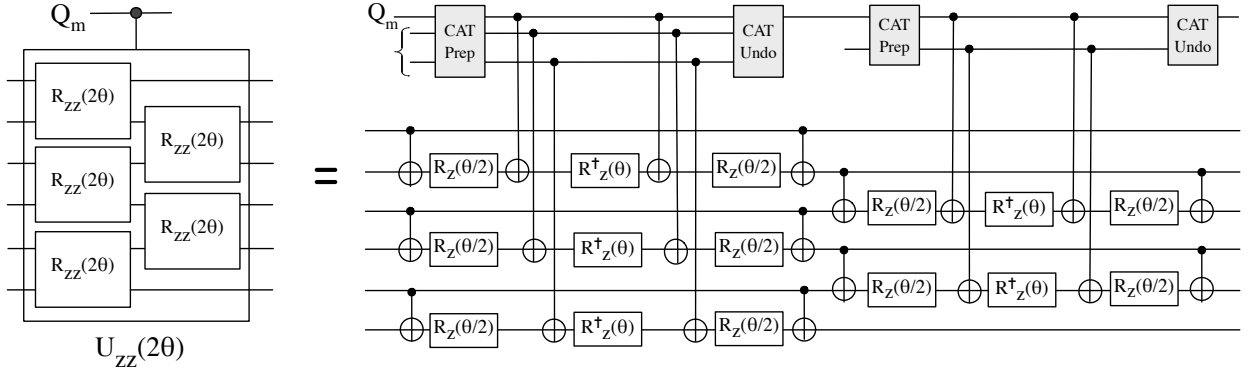


FIG. 5: The decomposition of the controlled unitary operation $U_{zz}(2\theta)$ gate into single-qubit R_z gates and CNOT gates.

additional qubits are used to prepare an N -qubit cat state (i.e., the state $|00\dots 0\rangle + |11\dots 1\rangle$) in order to parallelize each of the N $R_z(\theta)$ gates. The preparation of an N -qubit cat-state requires $(N - 1)$ CNOT gates. As can be seen in Figure 4, the implementation of the cat-state can be executed in parallel with the $R_z(\theta/4)$ gates. As shown later, the number of timesteps needed for the cat-state (i.e. $O(N)$) is several orders of magnitude less than the timesteps required to implement the $R_z(\theta/4)$ gate. Thus, the cat-state does not add any additional timesteps to the implementation of the circuit, but by parallelizing the controlled- $R_x(\theta)$ gates, it makes the number of timesteps to implement the circuit for the controlled- $U_x(\theta)$ independent on N .

The result of decomposing the controlled- $U_{zz}(2\theta)$ gate into single-qubit R_z gates and CNOT gates is illustrated in Figure 5 for $N = 6$. The two pairwise stages shown in Figure 3 for U_{zz} can be individually parallelized by adding $N/2$ and $N/2 - 1$ additional qubits prepared in a cat state. Each controlled- $R_{zz}(2\theta)$ gate is first expressed as a controlled- R_z gate and two CNOT gates (via the identity in Figure 6), and then further decomposed into four CNOT gates, and single-qubit $R_z(\theta/2)$ and $R_z^\dagger(\theta)$ gates.

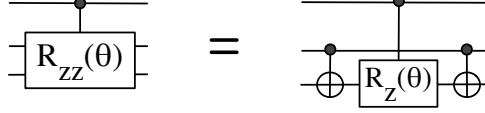


FIG. 6: Breaking-down the 3-qubit controlled R_{zz} gate into two-qubit gates.

Taken together, Figures 3, 4, and 5 show the decomposition of the controlled- $U(2^m \tau)$ into the controlled $U_x(\theta)$, $U_x(2\theta)$, and $U_{zz}(2\theta)$ gates, which are in turn decomposed into the CNOT gate, the H gate, and the three single-qubit gates $R_z(\theta)$, $R_z(\frac{\theta}{2})$, and $R_z(\frac{\theta}{4})$ for $\theta = \frac{2^m \tau}{k}$. Since the R_z gates cannot be implemented fault-tolerantly, each of them must be approximated as a sequence of T , S , and H gates via the Solovay-Kitaev algorithm to an accuracy of ϵ_{sk} where the length of the sequence scales as $O(\log^{3.97}(1/\epsilon_{sk}))$ [30]. The Solovay-Kitaev error is equivalent to a slight misrotation of the qubit. We numerically calculate the maximum overrotation that maintains the total error of the approximate unitary gate below the precision. We find that given a one qubit ϵ_{sk} and an N qubit ϵ_T , $Nk\epsilon_{sk} < \epsilon_T$.

Expanding Equation 8, as a function of the R_z gates (by substituting in the decompositions in Figures 4 and 5), shows that the number of computational timesteps necessary to implement the approximation of $U(2^m \tau)$ scales as $O(kS_R)$, where S_R denotes the length of each R_z sequence. Since there are M controlled unitary gates for $0 \leq m < M$, the total cost of the phase accumulation step in the TIM circuit scales as $\sum_m O(kS_R)$. Numerical calculations show that S_R is relatively independent of m for fixed M and N and is approximately 10^4 for $M \approx 10$ and $N \approx 40$.

C. Decomposing the Phase Measurement Step of the TIM Circuit

The third and final step of the phase estimation circuit is shown in Figure 2, which consists of the M -qubit inverse quantum Fourier transform (QFT) applied on the output register, followed by measurement of each of the M qubits. The circuit for an M -qubit inverse QFT (shown in Figure 7 for $M = 4$ qubits) consists of $O(M^2)$ gates and can be implemented in $2M$ timesteps. Each QFT timestep consists of one or more controlled- R_j operations, where R_j is a phase shift by $2\pi/2^j$ radians for $2 \leq j \leq M$. As described by Parker, et al. [31], it is possible to simplify the QFT circuit by distributing the M measurements of the output register in Figure 2 over a single control qubit that is reused for each measurement and replace the controlled- R_j gates with analogous single-qubit R_j gates. The resulting circuit for the TIM problem using a single control qubit as the output register is shown in Figure 8, which we use instead of Figure 2 in the resource analysis.

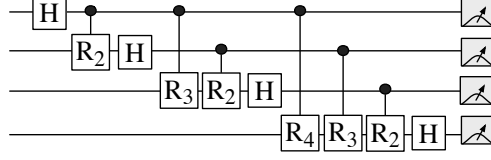


FIG. 7: Four-Qubit QFT Circuit.

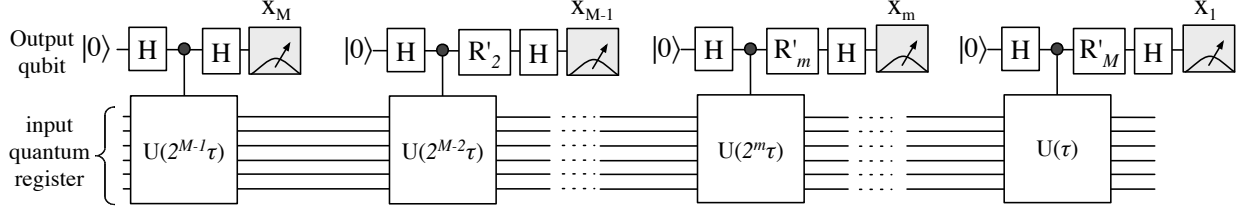


FIG. 8: An implementation of the phase estimation algorithm using one continuously recycled control qubit.

Each R'_m gate in Figure 8 is a sequence of m single-qubit R_z gates, corresponding to the m th sequence of controlled- R_j gates from the standard QFT circuit shown in Figure 7 [31]. Since each R_z gate must be approximated via the Solovay-Kitaev theorem, the number of timesteps needed to implement each R'_m is about mS_R . Thus the total number of timesteps necessary to implement the entire phase estimation circuit given in Figure 8 for the TIM problem scales as:

$$\sum_{m=0}^{M-1} [O(kS_R) + mS_R] = \sum_{m=0}^{M-1} O(kS_R) + S_RM^2 \quad (9)$$

where k scales as estimated in Equation 7. When using the circuit in Figure 8, the total number of qubits required for the TIM problem is $2N$. N qubits are needed for the input register, one qubit is needed for the output register, and maximum $(N - 1)$ ancillary qubits are needed for the cat-state used during the execution of each controlled unitary. In the next section, the physical resource requirements are calculated for the circuit in Figure 8, where each of the qubits is a logical qubit and each of the gates is a logical gate implemented fault-tolerantly.

IV. FAULT-TOLERANT ARCHITECTURE AND GATE DECOMPOSITION

The number of timesteps for the TIM problem and the total qubits required calculated in Section III reflect an application-level resource estimate for the TIM problem, without taking into account the underlying physical implementation of each gate and qubit. In this section, the quantum circuit is considered in

the context of fault-tolerant quantum error correction [8, 32, 33, 34] assuming the QLA architecture model. The effect of quantum error correction on the circuit’s resource requirements is two-fold.

- First, each qubit in the application circuit is a *logical* qubit, encoded into the state of a number of physical qubits. This encoding increases the total number of physical qubits needed.
- Second, each gate is a *logical* gate, realized via a circuit composed of physical gates applied on the logical qubits. This increases the number of physical timesteps required to implement each gate and may even require additional logical qubits.

Both the size of each logical qubit and the implementation of each logical gate depend on the performance parameters of the underlying physical technology, the type of error correcting code used, and the level of reliability required per logical operation. The level of reliability required is a function of the length of the overall computation and the total number of logical qubits necessary. The more logical qubits are used and the longer it takes to execute the application circuit, the more reliable each operation will need to be. For the specific instances of the TIM problem considered in Section V, the length of the computation (i.e. the number of logical timesteps given in Equation 9) is so large that the level of error correction necessary is equivalent to that for implementing the quantum factoring algorithm. A comparison between the resource requirements for the two applications is provided in Section V C.

The QLA architecture [35, 36] is the underlying logical architecture we use to analyze the resource requirements of the TIM problem in a fault-tolerant environment. The QLA is a tile-based, homogeneous quantum architecture design based on the ion-trap technology using surface electrode trap structures [37, 38, 39]. The QLA is explained in detail in the Appendix. Each tile in the QLA represents a single computational unit capable of executing fault-tolerantly any logical gate from the universal gate set given by:

$$\{H, \hat{\sigma}^n, P_T, P_S, \text{CNOT}, \text{Measure}\}, \quad (10)$$

where $\hat{\sigma}^n$ denotes the Pauli $\hat{\sigma}^x$, $\hat{\sigma}^y$, and $\hat{\sigma}^z$ operators. The gates P_T and P_S are used to initialize ancillary logical qubits needed for fault-tolerantly realizing the logical T and S gates. Upon application of the P_T and P_S gates, the ancilla qubits are placed in the states $T|+\rangle$ and $S|+\rangle$, respectively.

The QLA was originally designed and evaluated for Shor’s quantum factoring algorithm [40] for factoring up to 2048-bit integers. The error correction procedure used was a concatenated Steane $[[7, 1, 3]]$ quantum error correcting code [10]. To achieve the reliability necessary for factoring such large

integers, each logical tile in the QLA was designed to operate and store a level 2 logical qubit, which is composed of 7 level 1 logical qubits each encoded into the state of 7 physical ion-trap-based qubits. In this work, we had made some improvements in the design of the architecture, which include the use of the Bacon-Shor $[[9, 1, 3]]$ error correcting code [13, 41]. Additional details of the analysis of the architecture and the underlying logical qubit and operations design is provided in the appendix, including a detailed fault-tolerant threshold analysis for each logical operation and logical operation execution times.

In evaluating the performance of the TIM problem, we characterize the QLA architecture by two metrics. The quantity Q , denoting the number of computational tiles (i.e. logical qubits) and the quantity K , denoting the number of logical cycles required to execute the application circuit given in Figure 8. Since the fault-tolerant implementation of each logical operation in the QLA is dominated by error correction [35], a logical *cycle* is defined as time it takes to perform the necessary error correction on a logical qubit. Thus, the number of logical timesteps required to execute an application, given by Equation 9 for the TIM problem, can be divided into a number of logical cycles K , where many logical qubits may be undergoing a quantum operation during each cycle, with some operations requiring more than one logical cycle to complete. For example, the P_T and P_S gates in Equation 10 are implemented using two error correction steps [42] and thus, require two logical cycles. Similarly, any logical timestep which includes the T and S gates will require 6 logical cycles to complete [42], assuming the use of the P_T and P_S gates. As shown in the appendix, the real time duration of each QLA level 2 encoded logical cycle is approximately 0.07 seconds. Thus, the QLA architecture should be capable of executing 14 cycles per second, or $14Q$ logical operations per second, where Q is the total number of logical qubit tiles. In addition, each level 1 logical qubit requires 18 physical ion-trap-based qubits and each level 2 logical qubit requires approximately 1200 physical ion-trap-based qubits.

In the analysis, we also use the aggregate parameter, $KQ = K \times Q$ introduced in Reference [34]. An application is defined as executing successfully when the error probability per logical operation is less than $1/KQ$. Assuming a reasonable (if somewhat optimistic) physical ion-trap error probability of 10^{-7} per physical operation [43], an application with a KQ parameter of no greater 10^7 would require no error correction for successful execution. To determine how the KQ space changes with error correction a detailed analysis of the fault-tolerant threshold is necessary. In the Appendix for the QLA architecture and optimistic planar ion trap technology, a threshold of 1.7×10^{-6} is calculated. As a result, for a KQ value in the range 10^7 and 1.7×10^9 only level 1 error correction is necessary, for a range of 1.7×10^9 to 4.9×10^{12} level 2 error correction is required, and between 4.9×10^{12} and 4.1×10^{18} level 3 error correction would be needed.

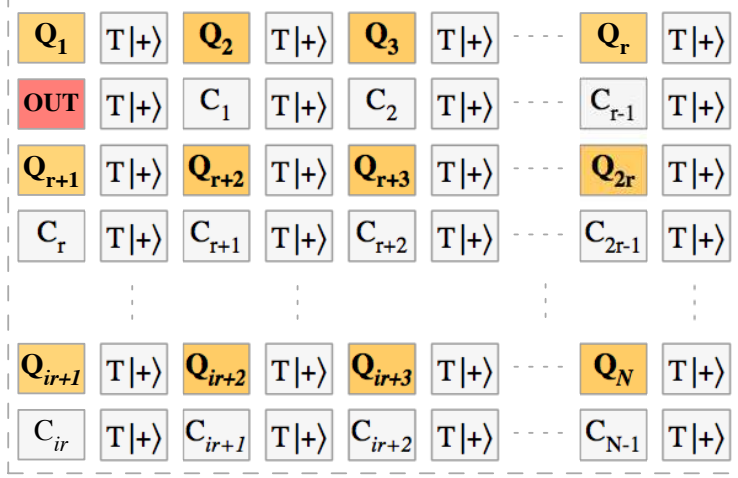


FIG. 9: QLA architecture for the TIM problem

To determine the TIM problem's Q parameter, the circuit shown in Figure 8 is mapped onto the QLA logical qubit tiles, where each tile represents a logical qubit. The tiles have four different functionalities. First, N logical qubit tiles are needed for the input register. Second, a single logical qubit tile is needed for the control qubit representing the output register. Third, $(N - 1)$ logical qubit tiles are required for the cat-state qubits, and finally, $2N$ auxiliary logical qubit tiles are included to enable implementation of the T or S gates. Thus, the N -qubit TIM problem requires $Q = 4N$ logical qubits to implement with the QLA architecture.

The resulting logical layout of the architecture is shown in Figure 10. The architecture is shown as a square grid of logical qubit tiles with $2r$ tiles per row and column, where r is approximately \sqrt{N} . The data input register tiles are labeled as $\{Q_1, Q_2, \dots, Q_N\}$. The output control qubit is labeled as OUT and the tiles labeled with $\{C_1, C_2, \dots, C_{N-1}\}$ are the cat-state logical qubits. Two ancillary $T|+\rangle$ tiles are used for each data tile to ensure that a prepared ancillary state is available when a T gate execution is required. As described in the appendix, S gates require only one logical cycle and no additional qubits at level 2 error correction to implement the code fault-tolerantly, but do require the additional qubits at level 1.

With $Q = 4N$ and K scaling as shown in Equation 9, the KQ parameter for the TIM problem scales as $O(2^M) + NM^2$ for a problem of size N and precision M . In Section V, it is shown that for a wide range of N and $M < 15$ this can be achieved using a level 2 EC code. For precision requirements of $M > 15$, level 3 error correction is necessary.

V. PERFORMANCE REQUIREMENTS ANALYSIS

In this section, the resource requirements for the 1-D TIM problem are calculated considering the fault-tolerant gate decomposition of the circuit given in Figure 8. More specifically, given a problem instance N and desired precision M , in Subsection V A, the logical cycles K , the number of logical qubits Q , and the level of error correction are numerically calculated assuming the QLA architecture. In addition, the resource requirements for the 1-D TIM problem are generalized to higher dimensions in Subsection V B and compare the resource requirements to those for implementing the quantum factoring algorithm in Subsection V C.

A. Performance requirements for the 1-D TIM problem

To calculate how many logical cycles are required to implement the 1-D TIM problem, given a specific problem instance N , we numerically calculate the following parameters for each controlled unitary $U(2^m\tau)$ for $0 \leq m < M$:

- The integer Trotter parameter $k \geq 1$, using the fact that the Trotter error ϵ_T must be less than the precision of the calculation $2\pi/2^M\tau$ given in units of energy.
- The Solovay-Kitaev sequences used to approximate $R_z(\theta)$, $R_z(\theta/2)$, and $R_z(\theta/4)$, for $\theta = (2^m\tau/2k)$, appearing in the decomposition of each $U(2^m\tau)$. The sequences are composed of H, T , and T^\dagger gates, where the T and T^\dagger gates require 6 logical cycles, as discussed in Section IV.

The results, described in more detail later in this section, indicate that the length of the computation for the ground-state energy is relatively large for several reasons. First, Trotterization of each controlled unitary is required and the Trotter parameter $k = O(2^m/N)$ increases exponentially with the desired precision M . Second, when error correction is necessary the number of logical timesteps (or cycles) increases for two reasons: (1) Within the implementation of each unitary $U(2^m\tau)$ the single-qubit R_z gates are approximated using the Solovay-Kitaev theorem; (2) Each timestep in the circuit execution is converted into one or more logical cycles, which requires many *physical* timesteps to complete due to error correction. Error correction increases the number of physical timesteps per logical cycle by a factor of $O(n^l)$, where n is a parameter of the error correcting code used and l is the level of error correction.

Consider, for example, the number of logical cycles K for $N = 40$, shown in Figure 10. The figure shows the behavior of K as a function of the desired precision $M \leq 20$, which corresponds to a maximum precision of 6 decimal digits. Considering that the y -axis scales logarithmically, the plot shows the

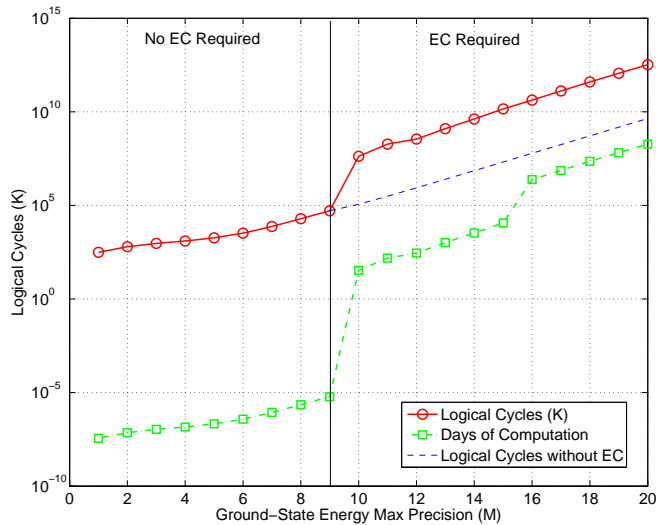


FIG. 10: Numerical calculations for the number of logical cycles K (red line) necessary assuming $N = 40$ spin TIM problem as a function of the desired precision $M \leq 20$. Estimate of the days of computation are shown with the lower dashed line.

exponential dependence of the length of the computation to the desired precision M , as influenced by the Trotter parameter k . In addition, the sudden increase in the length of the computation at $M \geq 10$ is due to the fact that error correction is required and the number of logical cycles suddenly increases due to the Solovay-Kitaev approximation sequences. As indicated in the figure, no error correction is required for $M < 10$, level 2 error correction is required for $10 \leq M \leq 15$ and level 3 error correction is required for $M \geq 16$.

The lower-most dashed line in Figure 10 shows the estimated length of the computation in real-time days rather than logical cycles K , assuming $10 \mu\text{s}$ physical gate times and the QLA architecture performance characteristics and underlying device technology, described in the appendix. Depending on the desired precision M , calculating the ground-state energy for the 40-spin TIM problem will require anywhere from a few seconds (for $M \leq 9$) to greater than 10^5 days ($M \geq 16$) to complete. The second sudden increase in the number of days required at $M = 16$ can be attributed to the need to employ level 3 error correction instead of level 2. This jump is not reflected in the number of logical cycles since the number of logical cycles does not reflect a change in the error correction level once error correction is required.

The results indicate that the length of the computation, as measured in logical cycles K or real-time days, is highly sensitive to both the desired precision M and the level of error correction required. The length of the computation is not affected by the problem size N for N smaller than the length of the Solovay-Kitaev

sequences. In particular, for each problem instance N , the number of logical cycles required remains relatively constant across fixed precision M , but increase or decrease as M changes. Thus, the precision M and not the problem size N has the greatest effect on the overall length of the computation.

B. Generalizing the 1-D TIM example to higher dimensions

While a 1-D TIM can be solved classically, a 2-D TIM with frustration cannot. However, the implementation of the quantum phase estimation circuit in Figures 2 or 8 is largely independent of the geometry of the N spin states and changes in the values of Γ_i and J_{ij} . For example, we consider Villain's model [44]. Villain's model is a 2-D square lattice where the rows have all ferromagnetic coupling and the columns alternate between ferromagnetic and antiferromagnetic. As discussed in Section III, the preparation of a ground state may be more difficult for a TIM but the calculation of the ground state energy increases by only a small factor.

Consider, for example, a square lattice with N spin sites, represented by N qubits in a $\sqrt{N} \times \sqrt{N}$ grid. The only change to the circuit for the phase estimation algorithm is the application of U_{zz} Ising interaction, which must be broken into two successive steps. First the rows of spin states are treated as the 1-D TIM problem in parallel, followed by the columns. Since the U_{zz} operations within each step are done in parallel, we still require $N/2$ additional qubits for the cat-states. Given that the rest of the operations, including the QFT implementation, remain the same, the increase in the number of timesteps to implement an N -spin 2-D TIM problem versus a 1-D TIM problem is by less than a factor of two. Similarly, the increase in the cost between a 1-D and a 3-D TIM problem will be by less than a factor of three. The effect on the fault-tolerance requirements and the architecture in implementing the 2-D TIM problem is that level 2 error correction will become necessary at precision $M = 10$ instead of $M = 11$.

C. Comparison of the TIM problem with Factoring using the QLA Architecture

The resource requirements necessary for the TIM problem are compared with those for implementing Shor's quantum factoring algorithm [40] using the QLA. While both applications employ the phase estimation algorithm, several differences in the requirements of each application are identified. First, the precision requirements between the two applications are different. For Shor's quantum factoring algorithm, the precision M must scale linearly with the size N of the N -bit number being factored [40], where N is as high

as 2048. On the other hand, the desired precision M is independent of the system size N for quantum simulations, and the application instances considered in this work $M \leq 25$.

The second difference lies in the implementation cost of the controlled unitary gates during the phase accumulation step for both application types. In Shor’s algorithm, the unitary is defined as $U(\tau)|x\rangle = |ax \bmod N\rangle$ and it can be shown that higher order powers of the unitary can be generated efficiently via modular exponentiation [28]. The result is that the implementation cost of $U(\tau)^{2^m}$ is equal to $2m$ times the implementation cost of $U(\tau)$. On the other hand, for generic quantum simulation problems, the implementation cost of $U(\tau)^{2^m}$ equals 2^m times $U(\tau)$, because of Trotterization. Thus, the implementation of the control unitary gates for quantum simulation is not as efficient as that for the modular exponentiation unitary gates.

A third important difference between the two applications is the creation of the input state $|\Psi\rangle$ and in initializing the input quantum register for the phase estimation algorithm. Any arbitrary state $|\Psi\rangle$ can be expressed as a superposition of the eigenvectors of the unitary $U(\tau)$: i.e., $|\Psi\rangle = \sum_i c_i |x_i\rangle$, where $|x_i\rangle$ is i th eigenstate, observed with probability $|c_i|^2$ via the phase estimation algorithm. If $|x_0\rangle$ is the ground-state energy eigenstate, then the closer the initial state $|\Psi\rangle$ is to $|x_0\rangle$, the more likely it is that the quantum simulation algorithm will succeed. On the other hand, for Shor’s Algorithm, the sum of the eigenvectors of the unitary $U(\tau)$ is simply the state $|\Psi\rangle = |1\rangle$, which is trivial to map onto the N -qubit input register. In addition, the eigenvalue corresponding to the majority of the eigenstates for the Shor unitary contains all that is necessary to calculate the factors of the number being factored.

Finally, factoring integers large enough to be relevant for modern cryptanalysis (i.e., $N = 1024$ bits or higher) requires several orders of magnitude more logical qubits than the scale of quantum simulation problems considered in this paper. At minimum, the factoring of an N -bit number requires $2N + 3$ qubits, using the same one-control qubit circuit given in Figure 8 [45]. As shown later, choosing to use only the minimum number of qubits required for factoring leads to high error correction overhead. A more reasonable implementation of the factoring algorithm requires $O(N^2)$ number of logical qubits, which is about 10^6 logical qubits for factoring a 1024-bit number. On the other hand, the quantum simulation problems we consider in this paper will require less than 500 logical qubits implemented on a real physical architecture.

Given the differences between these two applications, and the fact that they share the same underlying algorithm, we examine the relative size of the QLA architecture required implement either application. In particular, Figure 11 shows the performance of QLA-based quantum computers in KQ space with fixed physical resources. Each horizontal line corresponds to the KQ limit for a QLA-based architecture modeled

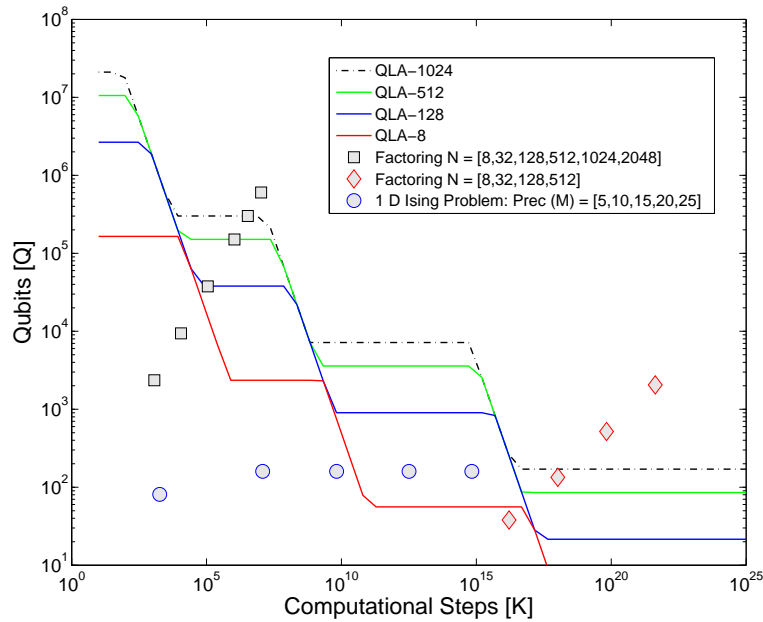


FIG. 11: Performance characteristics of different QLA-based quantum computers in KQ space with fixed amount of physical resources. The binary precision for the Ising problem of $M = \{5, 10, 15, 20, 25\}$ corresponds to decimal precision of $\{1, 3, 4, 6, 7\}$ digits, respectively.

for factoring a 1024-bit number (top-most horizontal dashed line), a 512-bit number, a 128-bit number, and an 8-bit number, respectively. The physical resources for each QLA- N quantum computer (where $N = \{1024, 512, 128, 8\}$ bits) are determined by how many logical qubits at level 2 error correction are required assuming the Quantum Carry Look-ahead Adder (QCLA) factoring circuit [35, 46], which requires $O(N^2)$ logical qubits and $O(N \log^2 N)$ logical cycles. The plateaus in each QLA- N line of Figure 11 represent using all of the qubits at a specific level of encoding, with the top-most right-hand plateau representing level 1. Where the lines are sloped, the model is that only a certain number of the lower level encoded qubits can be used. Once this reaches the number of qubits that can be encoded at the next level, the quantum computer is switched from encoding level L to $L + 1$ by using all the available level L qubits.

Figure 11 shows that a QLA- N quantum computer is capable of executing an application using level L encoded qubits if the application instance is mapped *underneath* the line representing the computer at level L . Factoring a 1024-bit number, for example, falls directly on the level 2 portion of the QLA-1024 line (see the square markers). Anything above that line cannot be implemented with the QLA-1024 computer. Similarly, factoring a 128-bit number maps under the QLA-128 line, but can be accomplished using level 1 qubits. The TIM problem is mapped onto Figure 11 for $N = 40$ and several binary precision instances: $M = \{5, 10, 15, 20, 25\}$, labeled with the circular markers. As expected, factoring requires many more

logical qubits, however, both applications require similar levels of error correction. A decimal precision of up to 4 digits of accuracy ($M = 15$) can be reached by using a quantum computer capable of factoring an 8-bit number at level 2 error correction, however higher precision quickly requires level 3 error correction.

The cost of implementing quantum factoring with one-control-qubit was calculated following the structure of Figure 8, with the unitary gates replaced with the modular exponentiation unitary gates. The results are shown with the diamond-shaped markers in Figure 11. While this particular implementation is the least expensive factoring network in terms of logical qubits [45], the high precision requirement of $M = O(N)$ makes this network very expensive in terms of timesteps. In fact, the number of timesteps required pushes the reliability requirements into the level 4 and above for factoring even modestly-sized numbers.

VI. CONCLUSION

In this paper, the TIM quantum simulation circuit was decomposed into fault-tolerant operations and have estimated the circuit's resource requirements and number of logical cycles K as a function of the desired precision M in the energy. The analysis was based on the QLA architecture and underlying technology parameters of trapped ions allowing us to calculate both K , as a function of the level of error correction, and the total length of the computation T in real-time.

An example calculation for T in days is demonstrated in the lower dashed line of Figure 10, where $T = Kt$ for t being the time it takes to execute a single logical cycle on the QLA. Multiple levels of error correction are necessary (level 2 at $M = 11$ and level 3 at $M = 16$) as the precision increases. This results in a long-computational time even for modest precision requirements. For example, at $M = 16$ (equal to about 5 decimal bits of precision) level 3 error correction is required and the estimated time to implement the TIM problem circuit is approximately 6×10^3 years. This is high because K itself is very high (about 4×10^{10}) and the time per logical cycle t at level 3 error correction is approximately 5 seconds, assuming the characteristics of the QLA architecture. On the other hand, if error correction were not required, the Solovay-Kitaev approximation of the three R_z gates from Section III would not be necessary, and K would be about 6×10^7 . In addition, t would be equal to a single physical timestep, which is about $10 \mu\text{s}$ for the ion-trap technology. This would reduce the total time T to just over 10 minutes.

Unfortunately, the number of logical cycles K is large enough so that error correction *is* required for implementing the circuit in Figure 8. The reason K grows so much is due to its linear dependence on the Trotter parameter k , which scales exponentially with the maximum desired precision M . Improving K will require the use of different underlying quantum simulation algorithms or different ways to implement

the phase estimation algorithm itself that limits its dependence on k . In addition, the Ising Hamiltonian H_I is composed of two non-commuting terms given by the U_x and the U_{zz} operators. The linear dependence of the number of timesteps on k is due to the fact that these terms do not commute since the expanded Trotter approximation for $U(2^m\tau)$ cannot be reduced. However, there are many physical systems, whose Hamiltonians are composed of commuting terms, *e.g.* the classical Ising model. In those cases, Trotterization be unnecessary. In future work, we intend to generalize the calculations of the resource requirements to other physical systems and consider different ways to implement the phase estimation algorithm that limit its dependence on the Trotter formula.

Reducing the logical cycle time t in the QLA architecture may also be possible. Three key parameters that play a role in determining t : the single physical gate time t_p , the threshold failure rate p_{th} , and the underlying physical failure rate p_0 . Figure 12 shows how the total computational time T varies with these parameters. The initial parameters are at $M = 16$, where $p_{th} = 1.7 \times 10^{-6}$, $p_0 = 10^{-7}$, and $t_p = 10 \mu s$ (the values used in Figure 10). The figure calculates T for power of 2 changes in the parameters. As expected the total time decreases linearly as we decrease the logical cycle t_p , shown with the square markers. Decreasing the physical failure rate (starred markers) and increasing the threshold by a factor of 2 (diamond markers) during each iteration cause T to decrease quadratically whenever lower error correction is required, otherwise T remains constant from one iteration to the next. A single change in the error correction level from level 3 to level 2 occurs by increasing p_{th} by a single factor of 2 but there is no gain for additional changes. Decreasing p_0 while keeping everything else constant (starred markers) yields two changes in the error correction level.

The line with the circular markers in Figure 12 shows how T changes as we improve all of the parameters by a factor of 2 during each iteration. We see that to pass $T = 100$ days, a threshold failure rate of $p_{th} = 5.4 \times 10^{-5}$, physical failure rate of $p_0 = 3.1 \times 10^{-9}$, physical gate speed of about $t_p = 300$ ns, and level 1 error correction instead of level 3. It is not difficult to imagine that such underlying parameters for a future quantum architecture are possible as the technologies continue to improve. In addition, the three parameters that we have considered may have a practical cooperative effect. Improving the physical failure rate, for example, may lead to better threshold failure rate by allowing some of the underlying operations to be weighted against one another. Similarly improving the threshold failure rate, may require choosing a more efficient quantum error correcting code which may have fundamentally shorter logical cycle time t .

[1] R. Feynman, International Journal of Theoretical Physics **21**, 467 (1982).

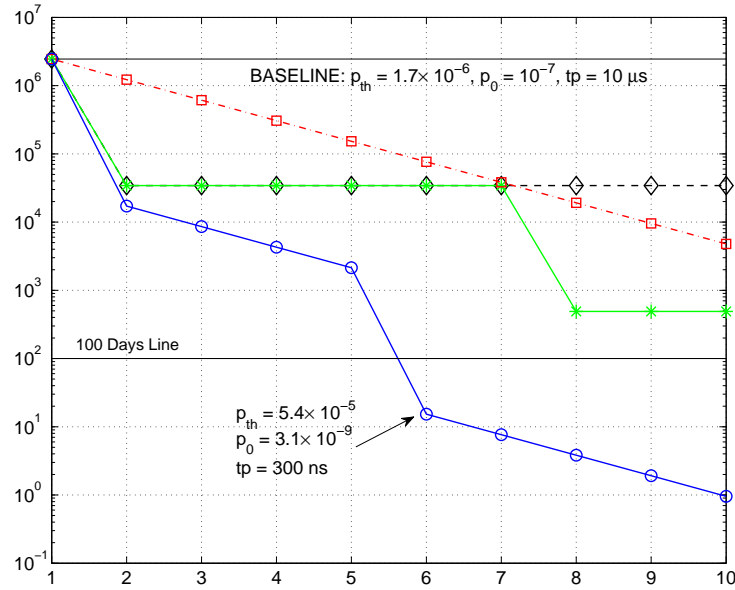


FIG. 12: The computation time T as we vary the physical cycle time t_p (square markers), physical failure rate p_0 (starred markers), threshold failure rate p_{th} (diamond markers), and all together (circular markers) by a factor of two during each iteration.

- [2] S. Lloyd, *Science* **273**, 1073 (1996).
- [3] D. Abrams and S. Lloyd, *Physical Review Letters* **79**, 2586 (1997).
- [4] D. Abrams and S. Lloyd, *Physical Review Letters* **83**, 5162 (1999).
- [5] C. Zalka, *Proc. R. Soc. Lond. A* **454**, 313 (1998).
- [6] A. Aspuru-Guzik, A. Dutoi, P. Love, and M. Head-Gordon, *Science* **309**, 1704 (2005).
- [7] I. Kassal, S. P. Jordan, P. J. Love, M. Mohseni, and A. Aspuru-Guzik (2008), arXiv:0801.2986v1.
- [8] P. Shor, in *Proceedings of the Symposium on the Foundations of Computer Science.*, IEEE (IEEE Press, Los Alamitos, CA, 1996).
- [9] D. Gottesman, in *Quantum Computation: A Grand Mathematical Challenge for the Twenty-First Century and the Millennium*, edited by J. S. J. Lomonaco (American Mathematical Society, Providence, Rhode Island, 2002), vol. AMS Short Course on Quantum Computation, pp. 221.
- [10] A. M. Steane, *Phys. Rev. Lett* **77**, 793 (1996).
- [11] D. Gottesman, *Journal of Modern Optics* **47**, 333 (2000).
- [12] A. M. Steane, *Phys. Rev. A* **68** (2003).
- [13] D. Poulin, *Phys. Rev. Lett.* **95**, 230504 (2005).
- [14] A. Y. Kitaev, A. H. Shen, and M. N. Vyalyi, *Classical and Quantum Computation*, vol. 47 of *Graduate Studies in Mathematics* (American Mathematical Society, Providence, 2002).
- [15] T. S. Metodi, D. D. Thaker, A. W. Cross, I. L. Chuang, and F. T. Chong, *ACM Journal on Emerging Technologies*

- in Computing Systems (JETC) **4** (2008).
- [16] P. Pfeuty, *Annals of Physics* **57**, 79 (1970).
- [17] R. J. Elliott, P. Pfeuty, and C. Wood, *Physical Review Letters* **25** (1970).
- [18] R. Jullien, P. Pfeuty, J. N. Fields, and S. Doniach, *Phys. Rev. B* **18**, 3568 (1978).
- [19] S. Sachdev, *Quantum Phase Transitions* (Cambridge University Press, Cambridge, England, U.K., 1999).
- [20] Moessner, R and Sondhi, S. L., *Phys. Rev. B* **68**, 054405 (2003).
- [21] Moessner, R and Sondhi, S. L. and Goerbig, M. O., *Phys. Rev. B* **73**, 094430 (2006).
- [22] Hu, Y. and Du, A., *J. Phys.:Condens. Matter* **20**, 125225 (2008).
- [23] M. Santos, *Phys. Rev. E* **61**, 7204 (2000).
- [24] A. Juozapavicius, S. Caprara, and A. Rosengren, *Phys. Rev. B* **56**, 11097 (1997).
- [25] J. Kempe, A. Kitaev, and O. Regev, *SIAM Journal of Computing* **35**, 1070 (2006).
- [26] J. Biamonte and P. Love, *Phys. Rev. A* **78**, 012352 (2008).
- [27] R. Cleve, A. Ekert, C. Macchiavello, and M. Mosca, *Proc. R. Soc. Lon. A* **454**, 339 (1998).
- [28] M. A. Nielsen and I. L. Chuang, *Quantum Computation and Quantum Information* (Cambridge University Press, Cambridge, UK, 2001).
- [29] M. Suzuki, *Phys. Lett. A* **165**, 387 (1992).
- [30] Dawson, C. M., Nielsen, M. A., *Quantum Information and Computation* **6**, 81 (2005).
- [31] S. Parker and M. Plenio, *Phys. Rev. Lett.* **85** (2000).
- [32] D. Aharonov and M. Ben-Or, *Proc. 29th Ann. ACM Symp. on Theory of Computing (STOC)* **29**, 176 (1997).
- [33] A. Y. Kitaev, 3rd Int. Conf. of Quantum Communication and Measurement pp. 181 (1997).
- [34] A. M. Steane, *Fortschritte der Physik* **46**, 443 (1999).
- [35] T. S. Metodi, D. D. Thaker, A. W. Cross, F. T. Chong, and I. L. Chuang (2005), proceedings of the 38th International Symposium on Microarchitecture **MICRO 38**.
- [36] D. D. Thaker, T. S. Metodi, A. W. Cross, I. L. Chuang, and F. T. Chong (2006), proceedings of the 33rd International Symposium on Computer Architecture **ISCA-33**.
- [37] J. Chiaverini, R. B. Blakestad, J. Britton, J. D. Jost, C. Langer, D. Leibfried, R. Ozeri, and D. J. Wineland, *Quantum Info. Comput.* **5**, 419 (2005).
- [38] J. I. Cirac and P. Zoller, *Phys. Rev. Lett.* **74**, 4091 (1995).
- [39] D. Wineland, M. Barrett, J. Britton, and J. C. et al., *Phil. Trans. R. Soc. Lond.* **A361**, 1349 (2003).
- [40] P. W. Shor, 35th Annual Symposium on Foundations of Computer Science pp. 124 (1994).
- [41] D. Bacon, *Phys. Rev. A* **73** (2006).
- [42] P. Aliferis, D. Gottesman, and J. Preskill, *Quantum Inf. Comput.* **6**, 97 (2007).
- [43] R. Ozeri, C. Langer, J. D. Jost, B. DeMarco, A. Ben-Kish, B. R. Blakestad, J. Britton, J. Chiaverini, W. M. Itano, D. B. Hume, et al., *Phys. Rev. Lett.* **95**, 030403 (2005).
- [44] Moessner, R and Sondhi, S. L., *Phys. Rev. B* **63**, 224401 (2001).
- [45] S. Beauregard, *Quantum Information and Computation* **3**, 175 (2003).
- [46] R. V. Meter and K. M. Itoh, *Phys. Rev. A* **71** (2005).

- [47] D. P. DiVincenzo, *Fortschritte der Physik* **48**, 771 (2000).
- [48] D. Kielpinski, C. Monroe, and D. J. Wineland, *Nature* **417**, 709 (2002).
- [49] J. Kempe, D. Bacon, D. A. Lidar, and K. B. Whaley, *Phys. Rev. A* **63** (2001).
- [50] W. Dur, H. J. Briegel, J. I. Cirac, and P. Zoller, *Phys. Rev. A* **59** (1999).
- [51] P. Aliferis and A. W. Cross, *Phys. Rev. Lett.* (arXiv:quant-ph/0610063) **98** (2006).
- [52] T. S. Metodi, D. D. Thaker, A. W. Cross, F. T. Chong, and I. L. Chuang, in *Proceedings of the SPIE Defense and Security Symposium, Orlando FL* **5** (2006).
- [53] K. M. Svore, D. P. DiVincenzo, and B. M. Terhal, *Quantum Inf. Comput.* **7**, 297 (2007).

APPENDIX A: THE QUANTUM LOGIC ARRAY ARCHITECTURE

This appendix offers an overview of the Quantum Logic Array (QLA) architecture model [35, 36] and our modifications to the model. The design of the QLA addresses several scalability issues that arise when considering large-scale quantum computers based on the circuit model of quantum computation. The scalability issues are summarized as follows:

- 1. Feasibility:** The system architecture must allow for the transition from a given technology with experimentally demonstrated quantum computing device components (qubits, gates, ..., etc.) to an actual physical installation that meets the DiVincenzo criteria [47] at the system level.
- 2. Reliability:** The system architecture must be designed to include the necessary physical resources given the underlying technology failure characteristics so that fault-tolerance can be achieved to maintain a minimum level of performance necessary to finish the application execution.
- 3. Communication efficiency:** A resource distribution protocol must be incorporated into the architecture design that allows quantum states to be transported over the desired distances with minimal auxiliary qubit resources and latency. We say that a communication protocol is efficient when there is an overlap between computation and communication, making the cost of communication negligible in terms of latency.

1. Physical Architecture

To address the issue of feasibility, we need a reasonable and detailed model of a large scale quantum computer that accounts for the physical interactions of the qubits. The QLA architecture is modeled with the ion trap quantum computing microarchitecture scheme proposed by Kielpinski, Monroe and Wineland (KMW) [48]. The KMW ion-trap microarchitecture scheme (illustrated in Figure 13) is based on using laser cooled ions as qubits and the shared motional states of ions in the same trap zone to perform conditional quantum gates. To perform communication between traps, the ions are physically shuttled from point to point by changing the trapping electric fields. All the basic components of this microarchitecture have been experimentally demonstrated, with some of the estimated physical trap performance parameters being: trap zone dimensions $100 \mu\text{m}$, ion movement speed 30 m/s , single-qubit gate failure rate 10^{-4} (in laboratory) and 10^{-7} assumed, two-qubit gate failure rate 3×10^{-2} (in laboratory) and 10^{-7} assumed, T_1 coherence time of years, and finally the T_2 dephasing time is 50 seconds. From a theoretical perspective all that is required is to put the pieces together and optimize gate fidelities to reach the assumed future gate fidelities. In reality, however, this remains as a daunting engineering task.

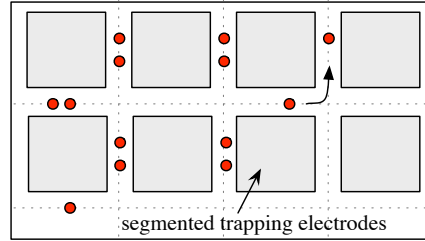


FIG. 13: The Kielipinski-Monroe-Wineland (KMW) Ion-Trap Microarchitecture

2. Logical Architecture

The QLA architecture is designed as a two-dimensional interconnected grid of computational tiles. Figure 14 shows a high-level view of a single tile. Each tile consists of the system-level logical qubit, a quantum repeater node (denoted with the letter R), and the system-level communication channel. The repeater node and the communication channel facilitate the communication between logical qubit tiles via quantum teleportation. The computational state of each level L logical qubit is encoded into the state of n_L lower-level qubits using an encoding scheme suitable for some $[[n_L, k, d_L]]$ quantum error correcting code. The error correcting code is capable of correcting errors in at most $(d_L - 1)/2$ lower-level qubits. The k parameter corresponds to the number of logical qubits represented by each encoding, which is assumed to be 1 in the QLA architecture.

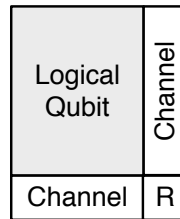


FIG. 14: High-level view of a QLA computational tile. The architecture is a 2D grid of tiles.

A logical qubit at level $L = 1$ is encoded into the state of a number of physical *ion-qubits*, where an ion-qubit is the physical embodiment of a level 0 qubit in the ion-trap technology. We assume that an ion-qubit is prepared using encoding techniques such as decoherence free subspace (DFS) (using one or more physical ions) to minimize correlated errors in the system [49]. The preparation of a suitable ion-qubit for concatenated quantum error correction is currently an open problem, however it may be possible to avoid DFS encoding schemes and use a single physical ion as the ion-qubit.

The QLA tiles divide into two functional types: computational tiles and storage tiles. Computational tiles include the physical resources (i.e. physical ion-qubits and communication channels) that are necessary

to store and error correct two logical data qubits at the highest level of encoding, including the necessary ancillary resources. The only logical operation on the data qubits in the storage tiles is the identity operation whose cost and failure probability depend on the length of time the data qubits spend between error correction steps and the type of error correction employed in memory. Design of the system architecture with separate memory and computational regions is discussed in Reference [36]. In such an architecture, one must consider the transfer mechanisms necessary between memory and computational tiles when two different encodings are used for storage and for computation, respectively. In this paper, we consider the original QLA architecture model [35], where every tile is a computational tile composed of the necessary resources to reliably implement any logical operation in a given universal gate set, followed by error correction. The universal gate set enabled by the QLA architecture is:

$$\{I, \hat{\sigma}_x, \hat{\sigma}_y, \hat{\sigma}_z, H, S, T, \text{CNOT}, M\}, \quad (\text{A1})$$

which contains the identity operator I , the Pauli operators $\hat{\sigma}_x$, $\hat{\sigma}_y$, and $\hat{\sigma}_z$, the Hadamard gate (H), the two-qubit controlled-NOT (CNOT) gate, the S gate which is a rotation of the qubit state by $\pi/2$ radians around the \hat{z} axis, the T gate, which is a \hat{z} rotation by $\pi/4$ radians, and finally, measurement (M) of a single qubit state.

Logical qubit tiles are connected via teleportation-based physical channels that utilize the Dur, et. al. quantum repeater scheme [50] tailored to the QLA architecture. The teleportation-based interconnect is discussed in detail in Reference [15], and is unmodified in our assumptions for this work.

3. Logical Qubits and Gate Resources

Fault-tolerant logical operations are implemented by first applying the logical gate network necessary to realize the state transformation of the encoded qubit, followed by error correction. The error correction step after each gate is necessary to ensure that any errors in the lower-level qubits accumulated during the gate do not propagate to the next logical gate [42]. Thus, a single QLA computational timestep is at least as expensive as the cost of error correction at the highest level of encoding.

At the highest level, logical qubits are encoded at level 2 into the state of 7 level 1 logical qubits, using the Steane $[[7, 1, 3]]$ quantum error cor

Each logical qubit tile contains the necessary resources to encode the logical qubit and to error correct it. The QLA architecture employs the Steane method of error correction, summarized in Figure 15, where

a minimum of two logical qubit blocks are required to store the data and the ancilla, respectively. To correct for Z errors, the ancilla is prepared in the logical $|0\rangle_L$ state and to correct for X errors the ancilla is prepared in the logical $|+\rangle_L$ state. After interaction with the data the ancilla is measured to extract the error syndrome. Additional ancilla blocks may be required to verify the preparation of the ancilla. The error correction network for the $[[9, 1, 3]]$ code is slightly simplified, where the 9-qubit logical ancilla that interacts with the data is divided into three blocks (each encoded separately) and interacted with three corresponding qubits from the data. In addition, the $[[9, 1, 3]]$ ancilla do not need to be verified with any additional ancilla qubits [51].

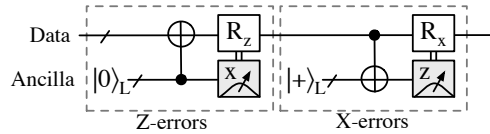


FIG. 15: A high-level view of the Steane method for quantum error correction. The R_z and R_x operations denote Z and X recovery, controlled on a measurement in the X or Z basis, respectively.

At level 1, the $[[7, 1, 3]]$ code requires at least three additional ancilla blocks to facilitate the ancilla preparation for either the logical $|0\rangle_L$ or $|+\rangle_L$ states [42]. In addition, one may choose to add additional ancillary resources to prepare multiple logical $|0\rangle_L$ or $|+\rangle_L$ states in parallel, and thus, speed up the error correction process. Since the $[[9, 1, 3]]$ code does not require verification of the ancilla we assume that one ancilla block is sufficient. Thus, a level 1 qubit implemented with the $[[7, 1, 3]]$ code requires at least 35 physical ion-qubits and a Bacon-Shor $[[9, 1, 3]]$ level 1 qubit requires 18 ion-qubits.

At level 2, each logical qubit is composed of seven level 1 qubits, necessary for the $[[7, 1, 3]]$ code. The entire level 2 QLA qubit tile, however, requires at least 70 level 1 logical qubit blocks, as shown in Figure 16 in order to accommodate all of the gates in Equation A1. Each level 2 qubit tile is designed to store two

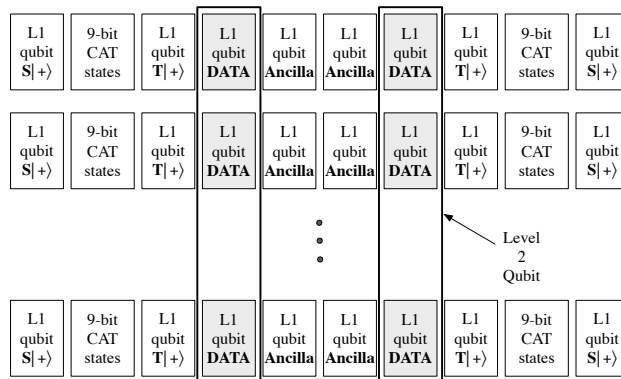


FIG. 16: Schematic of a Level 2 QLA Logical Qubit Tile

logical data qubits, each of which must have a level 2 ancilla (two middle columns of the tile) to facilitate error correction. In addition, the implementation of the T and S gates at level 1 requires level 1 ancilla tiles to store the logical $T|+\rangle_L$ and $S|+\rangle_L$ states, whose preparation requires 10 ion-qubits to prepare a 9-qubit CAT state. The total number of ion-qubits in a single level 2 tile is 1288 and (assuming existing planar trap dimensions [37]) the size of the tile can be as much as 0.03 mm^2 .

The networks for each logical gate can be transversal or non-transversal. Transversal gates are implemented by applying the equivalent gate on each of the lower-level qubits in parallel. Thus, the cost of each transversal gate is equivalent to a single physical gate-cycle, followed by the cost of error correction. The only non-transversal logical gates are the T gate for the $[[7, 1, 3]]$ code and the T and S gates for the $[[9, 1, 3]]$ code. The fault-tolerant implementation of non-transversal gates requires additional logical ancilla qubits prepared in the logical $T|+\rangle_L$ and $S|+\rangle_L$ states, respectively for the T and S gates.

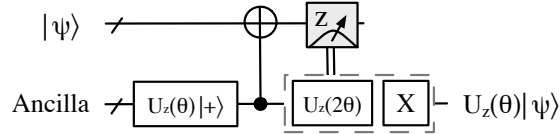


FIG. 17: Circuit used to implement fault-tolerantly the logical $U_z(\theta)$ gate (for T and S gates, $\theta = \{\pi/4, \pi/2\}$, respectively).

The circuit used to implement the T and S gates is shown in Figure 17, where the operator $U_z(\theta)$ refers to a rotation around the \hat{z} axis. For the T and S gates, θ is $\pi/4$ and $\pi/2$, respectively. Note that the T gate requires an S gate, which is transversal for the $[[7, 1, 3]]$ encoding, but will require another ancilla block for the $[[9, 1, 3]]$ encoding. The preparation of the logical $T|+\rangle_L$ and $S|+\rangle_L$ states requires an additional logical block encoded into a cat-state [42]. As shown in Figure 16, each tile contains enough resources to store two $|0\rangle_L$ or $|+\rangle_L$ states at level 2 prepared in parallel, which increases the probability that at least one of the states will be ready when needed.

The authors of the QLA architecture work did not provide detailed analysis of the performance and cost of each gate network type and did not consider the additional overhead from the implementation of the logical S and T gates. We consider this additional cost for a more accurate representation of the necessary resources to estimate the time of each logical timestep and the reliability achieved at level 2 encoding. In particular, we simulate each $[[9, 1, 3]]$ encoded level 1 logical network to determine its reliability and physical component threshold failure probability and use this information to extrapolate the performance of the $[[7, 1, 3]]$ encoded level 2 qubit tiles. The simulation takes into account physical ion-trap operations, such as movement, waiting, CNOT gates, single-qubit gates, measurement, and physical qubit initialization, as

required by the $[[9, 1, 3]]$ error correcting code. For each level 1 gate we derive a lower-bound of the fault-tolerant threshold using QASM-TOOLS, which is an open-source software suite for studying fault-tolerant quantum gates. We have modified QASM-TOOLS to accept quantum assembly language source files for each L1 gate automatically generated by the quantum physical operations scheduler QPOS [52]. QPOS is based on classical instruction scheduling heuristics and can be used to efficiently map any quantum circuit onto a physical grid to produce an assembly-level program reflecting the communication paths of the qubits, the maximal available parallelism, and the available classical resources (such as the communication channels).

Note that the network for the non-transversal T and S gates (Figure 17) decomposes into a number of transversal logical gates and the ancilla preparation operations P_T and P_S for the $T|+\rangle_L$ and $S|+\rangle_L$ states, denoted as P_T and P_S , respectively. Thus, we can assume that the temporal duration of each computational timestep in the QLA architecture (i.e. fundamental time cycle) is defined by the cost of error correction at the corresponding level of error correction, where each timestep implements one of the following logical operations:

$$\{I, \hat{\sigma}_n, H, P_T, P_S, \text{MOVE}, \text{WAIT}, \text{CNOT}, M\}, \quad (\text{A2})$$

where M denotes measurement, $\hat{\sigma}_n$ denotes one of the three Pauli operators, and MOVE and WAIT denote a logical movement step and a logical wait cycle. The only exception to the cost of fundamental timecycles are the ancilla preparation operations P_T and P_S , which require two error correction steps [42] and about 10 additional cycles for the interaction between the ancilla and an additional cat state qubit. The duration (seconds) and the resources for each timestep at level 1 are summarized in Table I, including the fault-tolerant threshold for each gate estimated from simulation of the level 1 circuitry following the methodology in Reference [53] and the software tools described above. For the level 1 WAIT gate, we increased the ion-qubits' waiting time until the threshold approached the CNOT threshold. This allowed us to determine the maximum allowed waiting time per logical level 1 qubit (about $110 \cdot 10 \mu\text{s}$ timesteps) before level 1 error correction must be initiated. We have assumed that all qubit blocks are arranged in a line as shown in Figure 18 for level 1 and similarly in Figure 16 for level 2.

Note from Table I that the least reliable operation is the CNOT gate with the lowest ion-trap threshold estimate of 1.7×10^{-6} . This threshold value, however, is a lower-bound computed using the methodology in Reference [42] consisting of a combinatorial count of all pairs of operations that cause more than one error in the network. In addition, the threshold value reflects all of the lower-level physical ion-trap operations treated equally, including movement and waiting. In practice, operations are not equal and their frequency

TABLE I: Simulated Cost of each Timestep at Level 1. Gate times are calculated assuming $10\mu\text{s}$ physical ion-trap operations.

Level	Op.	Estimated Cost (sec.)	Moves	Waits	Gates	FT Threshold
1	Single/M	1×10^{-3}	100	370	80	1.1×10^{-5}
1	$T/S +\rangle$	2×10^{-3}	240	780	130	2.3×10^{-5}
1	CNOT	1×10^{-3}	120	390	80	1.7×10^{-6}
1	WAIT	2×10^{-4}	0	972	0	2.1×10^{-6}

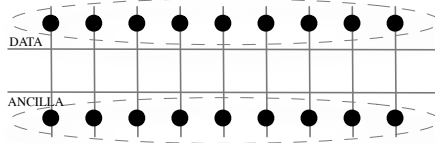


FIG. 18: Geometrical layout used to simulate logical qubits.

of usage varies. It is not unreasonable to assume that WAIT operations are several orders of magnitude more reliable than any logical gate. In fact, if we assume that WAIT operations are just a single order of magnitude more reliable than any other operation, the CNOT gate threshold increases to 9.3×10^{-6} , and the threshold values for all other gates are on the order of 10^{-4} . We use the threshold value of 1.7×10^{-6} to estimate the overall operation reliability at level 2 recursion using Gottesman’s analysis in Reference [11]. We estimate that the lowest reliability per operation is about 5×10^{-16} , which allows us to perform a computation with total system size KQ of about 2×10^{15} .

The estimated duration in seconds for each level 1 gate (third column in Table I) was obtained by taking into account that two error correction steps are performed after each gate instead of one. At least two error correction steps are necessary in the event of a non-trivial error syndrome to check that the non-trivial syndrome is correct, ensuring fault-tolerance [12]. Temporally, the most expensive operation is the T and S gates ancilla preparation, which takes 2 milliseconds at level 1, however, compilation techniques that map the application onto the device hardware will most likely overlap the ancilla preparation with other logical operations.

For level 2, the $[[7, 1, 3]]$ error correction network requires a total of 72 level 1 cycles comprising of about 90 total number of level 1 gates, 100 movement operations, and 425 level 1 waiting operations. Thus, a logical level 2 error correction procedure is approximately 0.07 seconds. The average waiting time between each two level 1 error correction steps during a level 2 error correction procedure is much smaller

than the maximum allowed waiting time of 110 timesteps. We find that the maximum allowed waiting time for level 2 qubits (i.e., time between error correction cycles) is about 0.1 seconds.